NANO LETTERS

pubs.acs.org/NanoLett

"Drawing with Nanotubes": Creating Nanowires with Complex Geometries by Pulsed Electrodeposition on Self-Organized Carbon Nanotube Patterns

Tohar S. Yarden and Ernesto Joselevich*

Department of Materials and Interfaces, Weizmann Institute of Science, Rehovot 76100, Israel

ABSTRACT We present a new approach for the creation of nanowires with well-defined complex geometries by electrodeposition onto self-organized single-walled carbon nanotubes. The concept is demonstrated by generation of continuous Au nanowires with various geometries, including parallel arrays, serpentines, and coils. The generality of this approach is further illustrated by synthesizing Bi_2Te_3 nanowires. Our concept of "drawing with nanotubes" offers to combine different material properties with complex geometries on the route to new functional nanosystems.

KEYWORDS Nanotubes, nanowires, self-assembly, electrodeposition, patterning, bismuth telluride

Envisioned nanodevices employ nanowires for various functions, such as semiconducting transistor channels and electrical interconnects.[1,2] Nanowires can also exhibit unique properties owing to their low-dimensionality, including electroluminescence,[3] lasing,[4] photoconductance,[5] thermoelectricity[6] and giant magneto-resistance.[7] Although research into nanowire synthesis has led to the development of extensive methods and encompassed numerous types of materials,[8] the process of device fabrication still poses major questions. Importantly, how can nanowires be shaped into desired geometries (e.g., curves, rings, etc.) or arranged according to specific designs? Self-assembly holds promising prospects for directed synthesis and organization:[9−12] It does not suffer from inherent resolution limits (as opposed to photolithography), while offering a parallel-process alternative to existing serial high-resolution processes (e.g., electron-beam lithography and SPM lithography).[13] For instance, careful control of nanowire growth conditions results in various complex geometries including helical,[14] ring,[15] kinked[16] and hyperbranched[17] nanowires. Templating is another method for synthesizing nanowires with different geometries.[18−23] Extensive efforts have been devoted to the use of biological molecules as nanowire or nanoparticle-array templates.[24−29] Nanowire arrays of different materials have been produced by electrodeposition onto step edges of highly ordered pyrolytic graphite (HOPG).[30−33] Single-walled carbon nanotubes have also been used as templates, though mainly for the chemical,[34,35] electrophoretic[36] and electrochemical deposition of nanoparticles.[37−42] Templating of continuous nanowires by nanotubes was reported on multiwalled nanotube forests[43−45] and on two-dimensional random networks of single-walled carbon nanotubes,[38] in both cases achieved by electrodeposition. However, templating of continuous nanowires on single-walled carbon nanotubes with well-defined geometries has not yet been reported, to the best of our knowledge. Our group has recently developed a new approach of "nanotube epitaxy"[46] whereby carbon nanotubes can be grown in a variety of self-organized patterns directed by surfaces, including parallel arrays,[46,47] grids,[48] serpentines, and coils.[49] This makes carbon nanotubes an attractive template for the deposition of nanowires. Here we show that single-walled carbon nanotubes with various complex geometries can be used as templates for the electrodeposition of nanowires of different materials, thus offering variety in both form and material of the products. Despite previous reports and common intuition,[39] we show that under certain conditions continuous coverage of the single-walled carbon nanotubes is not limited by nucleation on their relatively defect-free sidewall, but by diffusion limitation in a progressive nucleation mechanism. We overcome the diffusion limitation by using pulsed electrodeposition. This leads to the successful electrodeposition of continuous nanowires onto single-walled carbon nanotubes with well-defined complex geometries.

Our templating method is illustrated in Figure 1. Self-organized growth of single-walled carbon nanotubes is followed by electrodeposition from solution, in which the nanotubes function as working electrodes. We call this approach "drawing with nanotubes", because it creates nanowires with specific shapes and materials drawn with nanotubes, similar to lines drawn by an artist.

* To whom correspondence should be addressed. E-mail: ernesto.joselevich@weizmann.ac.il.

Received for review: 09/16/2010
Published on Web: 10/19/2010

DOI: 10.1021/nl103270s | *Nano Lett.* **2010,** *10,* 4742–4749

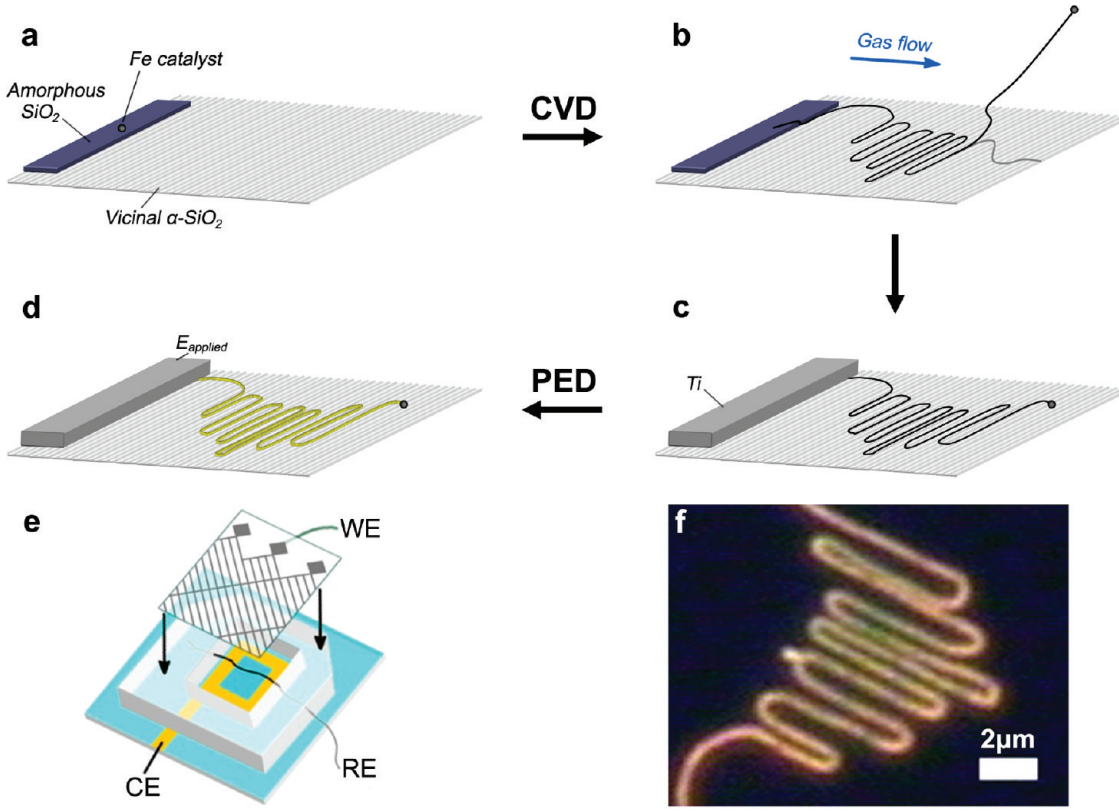

FIGURE 1. "Drawing with nanotubes" concept and realization. (a) Stripes of amorphous SiO_2 with Fe catalyst are patterned on a vicinal quartz substrate. (b) Carbon nanotube growth by chemical vapor deposition (CVD). The nanotubes grow and self-organize into patterns determined by surface features and gas flow. (c) Electrodes (Ti) are patterned on top of the amorphous SiO_2/Fe stripes to provide electrical contact with the nanotubes. (d) Au plating by pulsed electrodeposition (PED) from a solution of $HAuCl_4$. Au nanoparticles form and merge along the nanotubes as recurrent potential pulses are applied to them. (e) Illustration of the electrochemical cell for electrodeposition on carbon nanotubes. The Au counter electrode (CE) is patterned on a glass slide. The cell compartment is carved from a piece of polydimethylsiloxane and sewn through with a Ag wire, which is oxidized to Ag/AgCl and serves as a pseudoreference electrode (RE). The working electrode (WE) consists of carbon nanotubes grown on quartz and contacted by Ti electrodes. The transparent quartz substrate allows for real-time observation of the deposition process under an optical microscope. (f) Optical image of a serpentine Au nanowire templated by a self-organized nanotube.

The self-organization processes that we employ are surface-directed growth and nonequilibrium self-organization of single-walled carbon nanotubes, both developed in our group.[46,47,49] Arrays of parallel, straight nanotubes form along the surface steps of miscut sapphire[46] or quartz[50] when the catalyst for nanotube growth is patterned directly on the surface. This is due to the strong adhesion of growing nanotubes to the surface steps, nanofacets, or atomic rows of the substrate. Serpentines and coils are formed by depositing the catalyst on stripes of thin amorphous SiO_2, which causes nanotubes to grow upward from the surface.[49] These nanotubes then fall in a meandering or coiling pattern, similar to falling spaghetti, due to surface adhesion. Surface features (e.g., steps, nanofacets) introduce order into these patterns, resulting in regular, highly periodic serpentines.

The templating process used in this work is electrodeposition from solution, which exploits the electrical conductivity of carbon nanotubes, thus providing high selectivity (as quartz substrates are electrical insulators) and applicability under mild conditions compatible with other processes. Most importantly, its generality makes the concept of "drawing with nanotubes" applicable to various materials (metals, semiconductors, electropolymers) and different nanotube patterns (e.g., grids, serpentines, coils, etc.).

As a proof-of-concept, we demonstrate the electrodeposition of Au on carbon nanotubes with self-organized complex geometries. The materials and methods used in this work are described in detail in the Supporting Information. Briefly, carbon nanotubes are grown by chemical vapor deposition (CVD) on miscut quartz substrates and then contacted by photolithographic patterning of Ti electrodes. Au is deposited from $HAuCl_4$ 0.24 mM solution with a KCl 0.1 M supporting electrolyte. Potentials are given versus a Ag/AgCl pseudoreference electrode. The electrochemical cell is transparent to allow real-time observation under an optical microscope. Figure 1 shows an illustration of the experimental setup, together with an optical image of a templated nanowire.

The suitable potential range for Au electrodeposition was found using cyclic voltammetry (CV) while observing the sample under the optical microscope. Figure 2a shows a cyclic voltammogram for arrays of surface-aligned carbon

DOI: 10.1021/nl103270s | *Nano Lett.* **2010,** *10,* 4742–4749

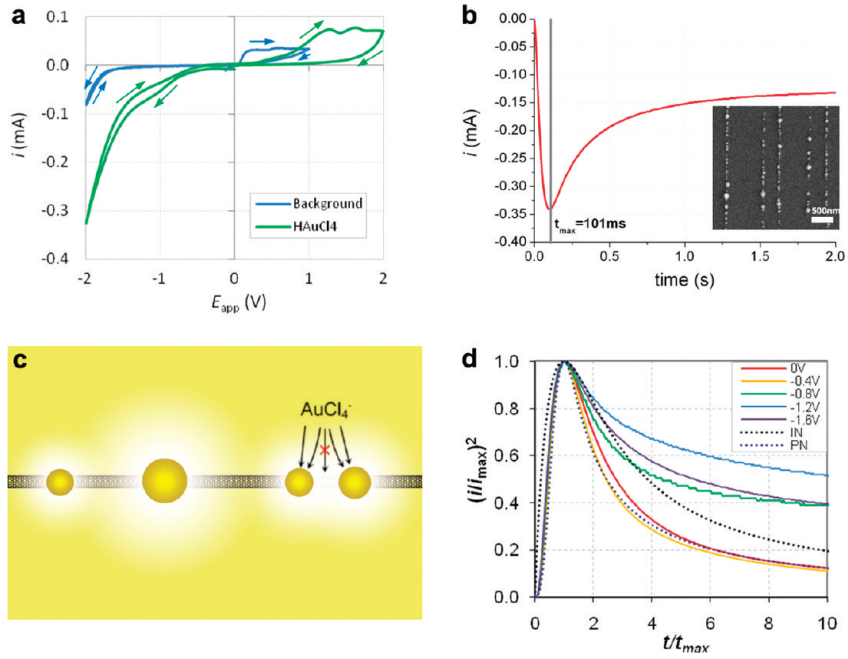

FIGURE 2. Electrochemical characterization of the Au electrodeposition on single-walled carbon nanotubes. (a) CV for surface-aligned single-walled carbon nanotubes, showing a reduction wave around −1.0 V and a stripping (oxidation) peak around 1.3 V (potentials vs Ag/AgCl). CV was performed in a solution of $HAuCl_4$ 0.24 mM, KCl 0.1 M (sweep rate 150 mV/s). (b) Current transient response to a potential step of −1.6 V in the same solution. Maximum current is reached at t_{max} = 101 ms. Constant potential steps on surface-aligned nanotubes only yield deposition of nanoparticles. SEM inset shows Au nanoparticles formed during 10 s of −1.6 V applied potential (scale bar 500 nm). (c) Illustration of diffusion effects around growing particles. Existing particles deplete reactive species around them as they grow, leading to the formation of "exclusion zones", where further nucleation is inhibited. The figure shows particles along a nanotube and the concentration gradients formed around them, represented by color gradients. Arrows represent diffusion of reactive species, showing how fewer particles can reach the interparticle section of the nanotube (the diffusion perpendicular to the surface should follow a similar pattern). (d) Qualitative assessment of the nucleation mechanism following the Scharifker−Hills method.[58] Dimensionless current transients are plotted for different potentials (solid lines) together with the theoretical curves (dotted lines) for instantaneous and progressive nucleation (IN and PN, respectively).

nanotubes in $HAuCl_4$ solution. Deposition of nanoparticles begins around 0.2 V with more nanoparticles appearing as potentials become more negative. It is selective to the carbon nanotubes, that is, nucleation over the quartz surface or Ti electrodes is insignificant. Stripping of the deposit was observed at positive potentials.

On the basis of the CV, we applied single potential steps from −0.2 to −1.6 V to surface-aligned nanotube arrays. However, single potential steps did not result in continuous coating of the nanotubes. Potential steps only promoted nucleation and growth of separate nanoparticles (Supporting Information Figure S1). Longer step durations increase the particle density (especially at less negative potentials), but mostly result in larger particles (10 s steps produce diameters larger than the desired wire thickness). Particle sizes are polydispersed. Higher particle densities are obtained by applying more negative potentials. The inset in Figure 2b shows the nanoparticles produced by a potential step of −1.6 V and 10 s. Differences in particle density among nanotubes were only observed for potential steps equal to or less negative than −1.0 V. Such differences may be attributed to the diameter and chirality distribution, since the rate of electron-transfer could depend on the electronic properties of the nanotube.[44] In addition, large contact resistances may arise due to Schottky barriers when the Fermi level is inside the bandgap of semiconducting nanotubes, leading to a smaller potential drop at the nanotube-solution interface.

Electrodeposition of Au on nanotubes appears to be limited by diffusion rather than by electron-transfer. This finding is based on three observations: (i) The inverse relationship between particle density and sizes. (ii) The particle morphology tends to be rough and is especially fractal-like at less negative potentials, as commonly seen in diffusion-limited aggregation (Supporting Information Figure S1). (iii) The decay of the potentiostatic current transients (Figure 2b) is typical of diffusion-limited reactions. Our finding adds to accumulating evidence of electrochemical activity of the carbon nanotube sidewalls, namely high electron-transfer rates at sidewalls[51,52] and patterns of metal deposition along carbon nanotubes.[37,38] Also, although selective nucleation at structural defects of carbon nanotubes has been shown in the past,[39] our Raman measurements found no signature of such defects along entire nanotube serpentines grown in our lab.[49]

We obtain significantly lower particle densities on surface-aligned nanotubes as compared to those reported in the literature for random nanotube networks.[37,38] The highest

DOI: 10.1021/nl103270s | Nano Lett. 2010, 10, 4742–4749

densities occur on nanotubes or nanotube segments that are not aligned by the surface. A single potential step could thus produce continuous Au nanowires on flow-aligned nanotubes. These nanotubes were aligned by gas flow to fall perpendicular to the quartz surface steps, to investigate the effect of surface alignment on nucleation (see Supporting Information Figure S2). We suspect that the properties of nanotubes may be altered by an anisotropic substrate effect, leading to significantly lower nucleation densities on surface-aligned carbon nanotubes. Possible substrate effects include physical deformation,[53,54] changes in electronic structure due to the direction of adsorption,[55] or an effect of the substrate on nanotube chirality during growth (as of yet reported only for sapphire).[56]

Nanotube serpentines exhibit another interesting pattern of electrodeposition, which may be substrate-induced. While some serpentines are uniformly decorated by Au nanoparticles following a potential step, others show decoration that is selective to the straight segments (Supporting Information Figure S3). An effect of surface alignment on the band structure of nanotube serpentines has in fact been shown by our recent Raman measurements.[57] In serpentines that are inherently semiconducting, the bottom sides of straight segments appear to acquire a metallic character. Thus, both electrochemical and Raman data suggest that the direction of alignment on the substrate can have an effect on the electronic properties of carbon nanotubes.

The diffusion limitation, coupled with low nucleation densities (which are especially low on surface-aligned nanotubes), thus seem to constitute a major obstacle for the electrodeposition of continuous nanowires on single-walled carbon nanotubes. As schematically explained in Figure 2c, under diffusion limitation the concentration of reactive species around each growing nucleus is depleted, which creates a growing "exclusion zone" in which no further nucleation can take place.[58,59] The appearance of new particles between existing ones is therefore inhibited. Thus, the diffusion limitation may be setting an upper limit for the nucleation density along nanotubes (a certain "saturation density"). This saturation density is lower than the nucleation site density inherent to the nanotube sidewalls. Note that our reasoning is based on the observation that the appearance of particles along nanotubes is indeed gradual, as seen under the optical microscope. The fact that the major obstacle is due to diffusion limitation and is not inherent to the properties of the single-walled carbon nanotubes leaves room for significant improvement of the electrodeposition by simply changing the profile of the applied potential. In the following section, we describe how a better understanding of the reaction kinetics assists us in obtaining higher nucleation densities and eventually continuous nanowires.

First, we ascertained that the gradual appearance of particles observed under the optical microscope indicates a mechanism of progressive nucleation (PN) for the electrodeposition of Au on single-walled carbon nanotubes (i.e., gradual activation of nucleation sites along the nanotubes) rather than instantaneous nucleation (IN, where all the nucleation sites would be activated at once). This was done by analyzing the current transients according to the method of Scharifker–Hills.[58] Figure 2d shows dimensionless transients recorded for various potential steps, compared to the theoretical curves for instantaneous and progressive nucleation (eqs 1 and 2, where i, i_{max}, t, and t_{max} denote the current, peak current, time, and the time of peak current, respectively). For less negative potential steps (0 to −0.6 V), the current transients closely resemble those theoretically expected for progressive nucleation, both in the rise and the decay. For more negative potential steps (−0.8 to −1.6 V), the current initially follows the progressive nucleation curve but shows a different type of decay after reaching the peak.

$$\text{IN:}\left(\frac{i}{i_{max}}\right)^2 = \frac{1.9542}{t/t_{max}}\{1 - \exp[-1.2564(t/t_{max})]\}^2 \quad (1)$$

$$PN:\left(\frac{i}{i_{max}}\right)^2 = \frac{1.2254}{t/t_{max}}\{1 - \exp[-2.3367(t/t_{max})^2]\}^2 \quad (2)$$

We note that use of the Scharifker curves to assess the nucleation mechanism in our system should be done with caution, because they were formulated for random nucleation on surfaces,[58,59] whereas in our system, nucleation density is not random over the whole surface but highest along nanotubes and lower in any other direction. However, at less negative potentials, the nucleation density along nanotubes is relatively low and then the anisotropy becomes negligible. This can explain why the experimental transients in our one-dimensional systems for the less negative potential steps closely resemble the theoretical curves developed for random two-dimensional nucleation.

For the more negative potential steps, the decay profile is not the typical Cottrellian $t^{-1/2}$ decay observed in both instantaneous and progressive nucleation,[58−61] but rather around $t^{-1/7}$. This non-Cottrellian decay could result from different factors, such as the anisotropy of the nanotube arrays, evolution of nonplanar diffusion regimes (e.g., hemicylindrical diffusion to individual nanotubes), electron-transfer limitations, and nanoelectrode effects[62] (see Supporting Information for a more detailed discussion). Decay profiles similar to our $t^{-1/7}$ have been reported for electrodeposition of Ag and Ni on carbon nanotube networks and forests, respectively.[38,42]

Further support for progressive nucleation is provided by scanning electron microscopy (SEM) images, which show a wide distribution of particle sizes uncorrelated to their local density (Figure 2b inset, Supporting Information Figures S1

DOI: 10.1021/nl103270s | Nano Lett. 2010, 10, 4742–4749

and S2c). This indicates that particles start to grow at different times during the application of the potential step, as consistent with a progressive nucleation mechanism.

On the basis of the above considerations, we conclude that the electrodeposition of Au on single-walled carbon nanotubes in our system proceeds by a mechanism of progressive nucleation for all of the applied potentials, even though the current transients for the more negative potential steps are not adequately described by the existing theory. This finding is also consistent with previous results for the electrodeposition of Pt on nanotube networks, which was shown to proceed by progressive nucleation via a slow multistep reduction of $PtCl_6^-$.[40] The progressive nucleation of Au in our system could be a similar case, since the reduction of $AuCl_4^-$ is also a multistep process.

The fact that the electrodeposition of Au on single-walled carbon nanotubes in our system proceeds by a mechanism of progressive nucleation confirms the diffusion limitation illustrated in Figure 2c. This explains why a single step cannot lead to the formation of continuous nanowires due to the merging of exclusion zones. We find that this diffusion limitation can be overcome by allowing the concentration of $AuCl_4^-$ near existing Au nuclei to replenish for a certain period of time, before resuming the application of potential for further nucleation and growth. This process can be repeated for a number of cycles using pulsed electrodeposition.

Pulsed electrodeposition (PED) is a common method of promoting dense nucleation on surfaces.[63] It consists of applying multiple short potential steps (pulses) of electrodeposition, separated by intervals of a different potential at which no deposition occurs. Each interval allows for regeneration of reactive species in the exclusion zones around existing nuclei. Nucleation between existing particles is therefore possible during the next pulse. To the best of our knowledge, PED has not yet been applied to single-walled carbon nanotube electrodes. Figure 3a presents a scheme of the pulse program with its various parameters.

Parallel arrays of continuous Au nanowires are obtained by pulsed electrodeposition on perfectly aligned single-walled carbon nanotubes on quartz[50] (Figure 3c,d). To produce these arrays, we applied 20 pulses of −1.6 V, 0.2 s long, separated by 1.0 s intervals of −0.06 V. The current response to this program is shown in Figure 3b. SEM and atomic force microscopy (AFM) scans of resulting nanowires are presented in Figure 3c,d, respectively. The heights of these nanowires (measured by AFM) are 40−50 nm, while widths (estimated by SEM) are 80−100 nm. The Au nanowires are roughly hemicylindrical, based on these observations. Our reasoning in choosing the PED parameters is explained in the following paragraphs.

The pulse potential, E_{on}, was set at a large overpotential for the reduction of $HAuCl_4$ on nanotube arrays (based on the CV and the results of single potential steps). This provides

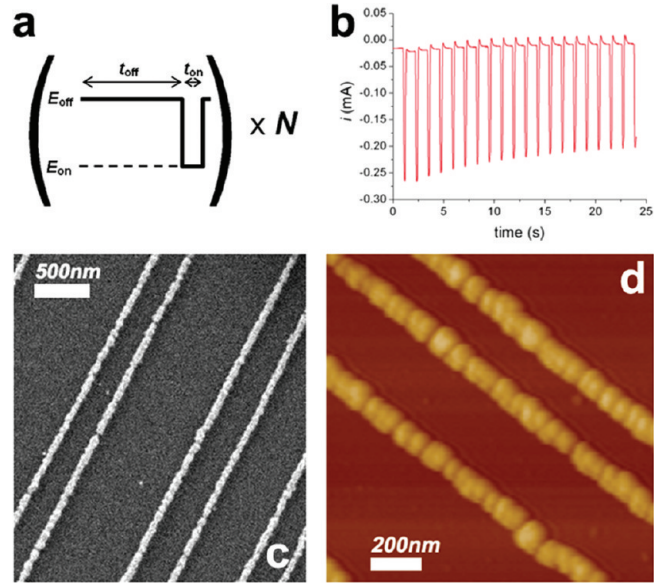

FIGURE 3. Continuous Au nanowires by pulsed electrodeposition (PED). (a) Diagram of the pulsed electrodeposition program. (b) Currents measured during PED of Au on surface-aligned nanotubes; $E_{on} = -1.6$ V, $E_{off} = -0.06$ V, $t_{on} = 0.2$ s, $t_{off} = 1.0$ s, and $N = 20$. (c) SEM and (d) AFM images showing arrays of parallel nanowires formed by PED. Nanowire heights in this image are around 40 nm.

a strong driving force for nucleation to compete with further growth of existing nanoparticles. The duration of each pulse, t_{on}, should allow near-saturation of the nucleation density but leave minimal time for particle growth. The time of peak current (t_{max}) marks the point when nucleation and growth are no longer significant due to diffusion limitations. The theory of nucleation on surfaces predicts that at t_{max}, the nucleation density reaches 95% of its saturation value.[58] We therefore set t_{on} as slightly longer than t_{max}.

For interval duration we initially choose $t_{off} \geq 3t_{on}$ and increase t_{off} if peaks of consecutive pulses show a marked decay. Such long intervals are required for diffusion to replenish the ion concentration near particles, but they make the choice of interval applied potential, E_{off}, crucial for the final thickness and continuity of the nanowires. E_{off} was chosen based on the CV as the point where, after the potential is swept to negative potentials and back (meaning that nucleation has occurred), the measured current is zero. Thus, no growth, shrinking, or stripping of existing particles should occur during t_{off}. The suitable number of repeats, N, was determined experimentally to obtain a minimum thickness of continuous nanowires.

Peak currents may be expected to increase rather than stay constant, since the surface area of the Au nuclei increases from one pulse to another. However, due to multiple nucleation on the surface, a regime of planar diffusion is rapidly attained, so the peak current is actually limited by the macroscopic area where the electrodeposition takes place. On the other hand, t_{max} becomes shorter from

DOI: 10.1021/nl103270s | Nano Lett. 2010, 10, 4742–4749

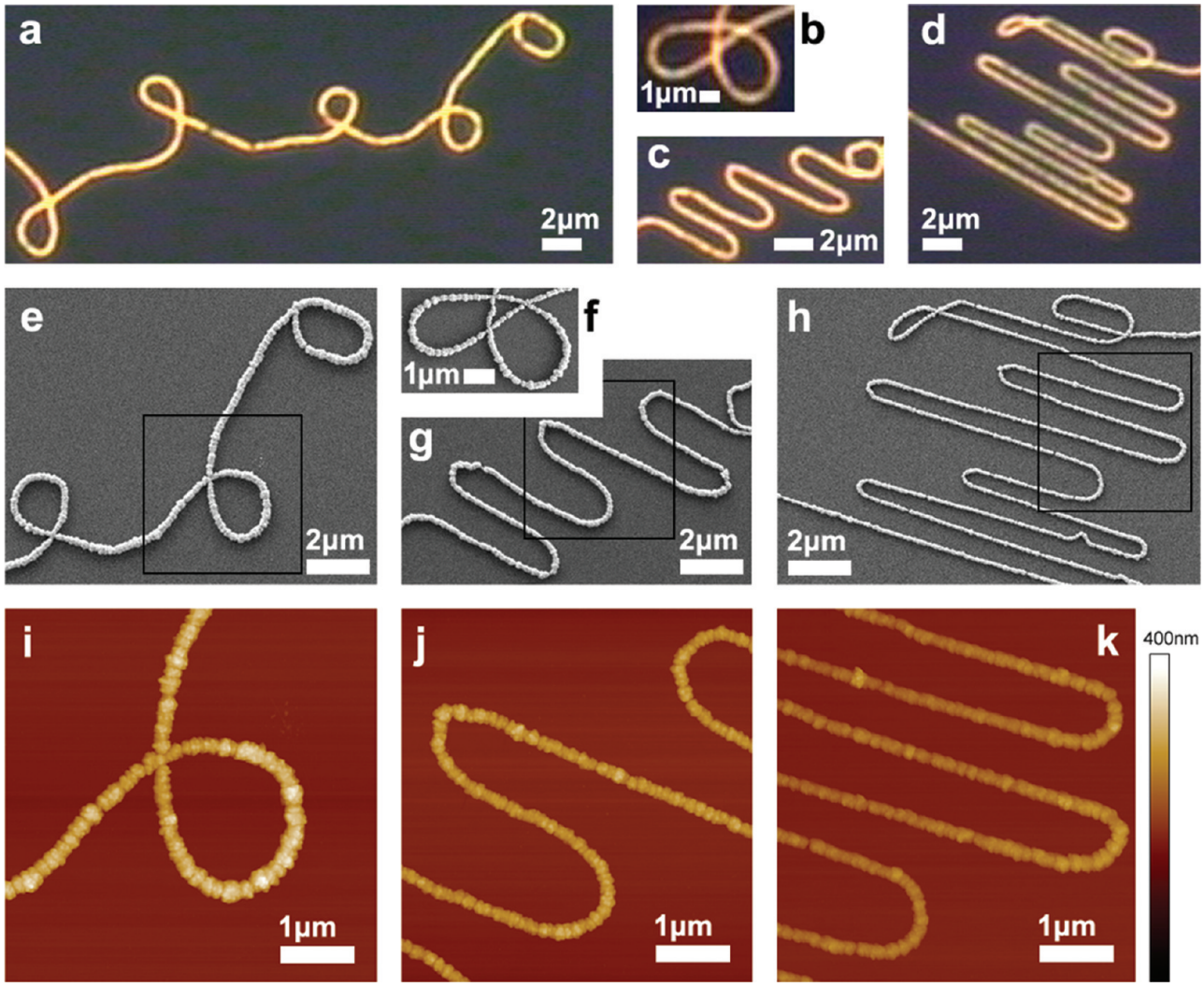

FIGURE 4. Au nanowires with complex geometries obtained by PED on self-organized carbon nanotubes. Images by optical microscopy (a−d), SEM (e−h), and AFM (i−k). Examples include a coil (a,e,i), a "pretzel" shape (b,f), and two serpentines (c,g,j and d,h,k). Black frames on the SEM images locate the sections whose AFM scans are presented below. AFM height measurements for (i) are 120−180 nm, for (j) 90−100 nm along the straight segments and up to 130 nm at the curved segments, and for (k) 75−90 nm along the straight segments and about 100 nm at the curved segments. Parameters of the PED program were $E_{on} = -1.6$ V, $E_{off} = -0.06$ V, $t_{on} = 0.2$ s, $t_{off} = 1.3$ s, and $N = 20$.

pulse to pulse due to increase in the microscopic nuclei surface area.

Serpentine and coiled Au nanowires were templated on self-organized carbon nanotube serpentines[42] and coils, respectively, using the same PED program as mentioned above, but applying longer intervals ($t_{off} = 1.3$ s). Optical, SEM, and AFM images of these nanowires are shown in Figure 4. Wire heights (measured by AFM) of serpentines at the straight segments are 80−90 nm, again suggesting a hemicylindrical cross-section. The curved sections of serpentine nanowires are thicker than the straight ones, with a height of about 120 nm. For coils, cross-section heights are between 120 and 180 nm. The difference in nanowire thickness between the straight and curved segments of the serpentines may be explained in two ways. (i) Curved sections grow larger because they have less competition for reactant species from neighboring nanotube segments. (ii) There could be some degree of selectivity for nucleation depending on nanotube alignment or curvature, as observed with single potential steps (Supporting Information Figure S3). As of yet, we cannot determine whether the thicker curved sections of Au serpentines result from either or both reasons.

We demonstrate the general applicability of our "drawing with nanotubes" concept to other materials by electrodepositing bismuth telluride (Bi_2Te_3) along surface-aligned nanotube arrays. Bi_2Te_3 is a room-temperature thermoelectric material exhibiting increased performance in low-dimensional structures (e.g., nanowires).[64,65] It can be electrodeposited from solution according to the following reaction:[66]

$$2Bi^{3+} + 3HTeO_2^{+} + 18e^{-} + 9H^{+} \rightarrow Bi_2Te_{3(s)} + 6H_2O \quad E^0 = 0.62V$$

DOI: 10.1021/nl103270s | *Nano Lett.* **2010,** *10,* 4742–4749

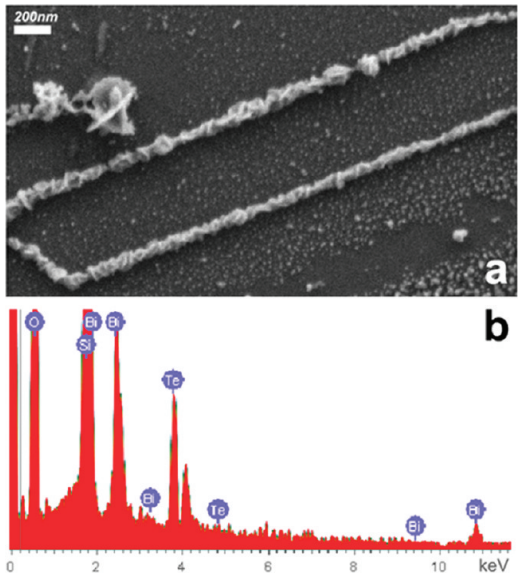

FIGURE 5. Electrodeposition of Bi_2Te_3 nanowires on carbon nanotube arrays. (a) Structures deposited on surface-aligned carbon nanotube arrays during two consecutive voltammetry cycles in a solution of $Bi(NO_3)_3$ 5 mM, TeO_2 6.67 mM, HNO_3 1.6 M (at 10 mV/s). The SEM image shows the dominant macle morphology (similar to intersecting platelets) forming continuous wires of ca. 100 nm width. (b) EDS spectrum for a large macle shape, similar but larger than those shown in (a). Elements detected are Si, O (which make up quartz), Bi and Te. The latter two were found at a ratio of 1:1.405, corresponding to a $Bi_2Te_{2.81}$ stoichiometry.

Figure 5 shows Bi_2Te_3 nanowires produced during cyclic voltammetry in a solution of $Bi(NO_3)_3$ and TeO_2. The Bi_2Te_3 nanowires are straight, parallel to each other and about 100 nm thick. The exact stoichiometry of the Bi_2Te_3 nanowires determined by energy-dispersion spectroscopy (EDS) is $Bi_2Te_{2.81}$, which is very close to the ideal Bi_2Te_3 stoichiometry within the measurement error range. This is the first demonstration of Bi_2Te_3 nanowires synthesized by templating onto carbon nanotubes.

In summary, we have shown that self-organized carbon nanotube patterns can serve as templates for the synthesis of Au nanowires with well-defined and complex geometries. Pulsed electrodeposition was used to obtain continuous nanowires on surface-aligned carbon nanotube arrays and also on carbon nanotube serpentines and loops. The geometries of the nanotube templates are inherited by the nanowires. We have demonstrated that our new concept of "drawing with nanotubes" can be generally applied to different materials by electrodepositing Bi_2Te_3 nanowires onto surface-aligned carbon nanotubes. More recently, we have also been able to produce CdSe nanowire serpentines by the same method.[67] We can envisage that thermoelectric and semiconducting nanowires with a serpentine geometry could in the future be used to create "nanorefrigerators", "nano-neon lights", ultrasensitive photodetectors, and all sorts of functional nanosystems combining the unique properties of different materials with self-organized complex geometries. Our method offers control over the shapes and spatial arrangements of nanowires of various materials. Such control is important for the integration of nanowires into functional systems.

Acknowledgment. We thank Dr. Alexander Vaskevich, Dr. K. S. Nagapriya, and Nitzan Shadmi for helpful discussions. This research was supported by the Israel Science Foundation, the U.S.-Israel Binational Science Foundation, the Kimmel Center for Nanoscale Science, and the Djanogly, Alhadeff, and Perlman Family foundations. We thank Professor Ron Naaman for use of his potentiostat.

Supporting Information Available. Materials and methods, images of Au deposition patterns on carbon nanotubes and discussion of current transient profiles. This material is available free of charge via the Internet at http://pubs.acs.org.

REFERENCES AND NOTES

(1) Wu, Y.; Xiang, J.; Yang, C.; Lu, W.; Lieber, C. M. *Nature* **2004**, *430*, 61–65.
(2) Lu, W.; Lieber, C. M. *Nat. Mater.* **2007**, *6*, 841–850.
(3) Nassiopoulos, A. G.; Grigoropoulos, S.; Papadimitriou, D. *Appl. Phys. Lett.* **1996**, *69*, 2267–2269.
(4) Huang, M. H.; Mao, S.; Feick, H.; Yan, H. Q.; Wu, Y. Y.; Kind, H.; Weber, E.; Russo, R.; Yang, P. D. *Science* **2001**, *292*, 1897–1899.
(5) Kind, H.; Yan, H. Q.; Messer, B.; Law, M.; Yang, P. D. *Adv. Mater.* **2002**, *14*, 158–160.
(6) Dresselhaus, M. S.; Lin, Y. M.; Rabin, O.; Jorio, A.; Souza Filho, A. G.; Pimenta, M. A.; Saito, R.; Samsonidze, G. G.; Dresselhaus, G. *Mater. Sci. Eng., C* **2003**, *23*, 129–140.
(7) Hong, K. M.; Yang, F. Y.; Liu, K.; Reich, D. H.; Searson, P. C.; Chien, C. L.; Balakirev, F. F.; Boebinger, G. S. *J. Appl. Phys.* **1999**, *85*, 6184–6186.
(8) Xia, Y. N.; Yang, P. D.; Sun, Y. G.; Wu, Y. Y.; Mayers, B.; Gates, B.; Yin, Y. D.; Kim, F.; Yan, Y. Q. *Adv. Mater.* **2003**, *15*, 353–389.
(9) Whitesides, G. M.; Grzybowski, B. *Science* **2002**, *295*, 2418–2421.
(10) Lehn, J. M. *Science* **2002**, *295*, 2400–2403.
(11) Wang, Y. H.; Mirkin, C. A.; Park, S. J. *ACS Nano* **2009**, *3*, 1049–1056.
(12) Lu, W.; Lieber, C. M. *Nat. Mater.* **2007**, *6*, 841–850.
(13) Gabai, R.; Ismach, A.; Joselevich, E. *Adv. Mater.* **2007**, *19*, 1325–1330.
(14) Zhang, H. F.; Wang, C. M.; Buck, E. C.; Wang, L. S. *Nano Lett.* **2003**, *3*, 577–580.
(15) Kong, X. Y.; Wang, Z. L. *Nano Lett.* **2003**, *3*, 1625–1631.
(16) Tian, B. Z.; Xie, P.; Kempa, T. J.; Bell, D. C.; Lieber, C. M. *Nat. Nanotechnol.* **2009**, *4*, 824–829.
(17) Zhu, J.; Peng, H. L.; Chan, C. K.; Jarausch, K.; Zhang, X. F.; Cui, Y. *Nano Lett.* **2007**, *7*, 1095–1099.
(18) Saito, M.; Kirihara, M.; Taniguchi, T.; Miyagi, M. *Appl. Phys. Lett.* **1989**, *55*, 607–609.
(19) Heremans, J.; Thrush, C. M.; Zhang, Z.; Sun, X.; Dresselhaus, M. S.; Ying, J. Y.; Morelli, D. T. *Phys. Rev. B* **1998**, *58*, 10091–10095.
(20) Zhang, Z. B.; Ying, J. Y.; Dresselhaus, M. S. *J. Mater. Res.* **1998**, *13*, 1745–1748.
(21) Limmer, S. J.; Seraji, S.; Forbess, M. J.; Wu, Y.; Chou, T. P.; Nguyen, C.; Cao, G. Z. *Adv. Mater.* **2001**, *13*, 1269–1272.
(22) Barbic, M.; Mock, J. J.; Smith, D. R.; Schultz, S. *J. Appl. Phys.* **2002**, *91*, 9341–9345.
(23) Lahav, M.; Sehayek, T.; Vaskevich, A.; Rubinstein, I. Nanoparticle Nanotubes. *Angew. Chem., Int. Ed.* **2003**, *42*, 5576–5579.
(24) Braun, E.; Eichen, Y.; Sivan, U.; Ben-Yoseph, G. *Nature* **1998**, *391*, 775–778.
(25) Keren, K.; Krueger, M.; Gilad, R.; Ben-Yoseph, G.; Sivan, E.; Braun, E. *Science* **2002**, *297*, 72–75.
(26) Keren, K.; Berman, R. S.; Buchstab, E.; Sivan, U.; Braun, E. *Science* **2003**, *302*, 1380–1382.

DOI: 10.1021/nl103270s | *Nano Lett.* **2010,** *10,* 4742–4749

(27) Le, J. D.; Pinto, Y.; Seeman, N. C.; Musier-Forsyth, K.; Taton, T. A.; Kiehl, R. A. *Nano Lett.* **2004**, *4*, 2343–2347.
(28) Park, S. H.; Yan, H.; Reif, J. H.; LaBean, T. H.; Finkelstein, G. *Nanotechnology* **2004**, *15*, S525–S527.
(29) Reches, M.; Gazit, E. *Science* **2003**, *300*, 625–627.
(30) Walter, E. C.; Murray, B. J.; Favier, F.; Kaltenpoth, G.; Grunze, M.; Penner, R. M. *J. Phys. Chem. B* **2002**, *106*, 11407–11411.
(31) Zach, M. P.; Ng, K. H.; Penner, R. M. *Science* **2000**, *290*, 2120–2123.
(32) Ji, X. B.; Banks, C. E.; Xi, W.; Wilkins, S. J.; Compton, R. G. *J. Phys. Chem. B* **2006**, *110*, 22306–22309.
(33) Menke, E. J.; Li, Q.; Penner, R. M. *Nano Lett.* **2004**, *4*, 2009–2014.
(34) Choi, H. C.; Shim, M.; Bangsaruntip, S.; Dai, H. J. *J. Am. Chem. Soc.* **2002**, *124*, 9058–9059.
(35) Qu, L. T.; Dai, L. M. *J. Am. Chem. Soc.* **2005**, *127*, 10806–10807.
(36) Zheng, L.; Li, S.; Burke, P. J. Self-assembled gold nanowires from nanoparticles: an electronic route towards DNA nanosensors. In *Nanoengineering: Fabrication, Properties, Optics, and Devices*; Dobisz, E. A., Eldada, L. A., Eds.; Proceedings of SPIE; SPIE: Bellingham, WA, 2004; pp 117−124.
(37) Quinn, B. M.; Dekker, C.; Lemay, S. G. *J. Am. Chem. Soc.* **2005**, *127*, 6146–6147.
(38) Day, T. M.; Unwin, P. R.; Wilson, N. R.; Macpherson, J. V. *J. Am. Chem. Soc.* **2005**, *127*, 10639–10647.
(39) Fan, Y. W.; Goldsmith, B. R.; Collins, P. G. *Nat. Mater.* **2005**, *4*, 906–911.
(40) Day, T. M.; Unwin, P. R.; Macpherson, J. V. *Nano Lett.* **2007**, *7*, 51–57.
(41) Qian, Y.; Huang, S. M.; Gao, F. L.; Cai, Q. R.; Zhang, L. J.; Hu, W. B. *J. Phys. Chem. C* **2009**, *113*, 6983–6988.
(42) Tamburri, E.; Toschi, F.; Guglielmotti, V.; Scatena, E.; Orlanducci, S.; Terranova, M. L. *J. Nanoparticle Res.* **2009**, *11*, 1311–1319.
(43) Gao, M.; Huang, S. M.; Dai, L. M.; Wallace, G.; Gao, R. P.; Wang, Z. L. *Angew. Chem., Int. Ed.* **2000**, *39*, 3664–3667.
(44) Chen, J. H.; Huang, Z. P.; Wang, D. Z.; Yang, S. X.; Wen, J. G.; Ren, Z. F. *Appl. Phys. A* **2001**, *73*, 129–131.
(45) Tang, H.; Chen, J. H.; Huang, Z. P.; Wang, D. Z.; Ren, Z. F.; Nie, L. H.; Kuang, Y. F.; Yao, S. Z. *Carbon* **2004**, *42*, 191–197.
(46) Ismach, A.; Segev, L.; Wachtel, E.; Joselevich, E. *Angew. Chem., Int. Ed.* **2004**, *43*, 6140–6143.
(47) Ismach, A.; Kantorovich, D.; Joselevich, E. *J. Am. Chem. Soc.* **2005**, *127*, 11554–11555.
(48) Ismach, A.; Joselevich, E. *Nano Lett.* **2006**, *6*, 1706–1710.
(49) Geblinger, N.; Ismach, A.; Joselevich, E. *Nat. Nanotechnol.* **2008**, *3*, 195–200.
(50) Kang, S. J.; Kocabas, C.; Ozel, T.; Shim, M.; Pimparkar, N.; Alam, M. A.; Rotkin, S. V.; Rogers, J. A. *Nat. Nanotechnol.* **2007**, *2*, 230–236.
(51) Heller, I.; Kong, J.; Williams, K. A.; Dekker, C.; Lemay, S. G. *J. Am. Chem. Soc.* **2006**, *128*, 7353–7359.
(52) Heller, I.; Kong, J.; Heering, H. A.; Williams, K. A.; Lemay, S. G.; Dekker, C. *Nano Lett.* **2005**, *5*, 137–142.
(53) Hertel, T.; Walkup, R. E.; Avouris, P. *Phys. Rev. B* **1998**, *58*, 13870–13873.
(54) Ding, L.; Zhou, W. W.; McNicholas, T. P.; Wang, J. Y.; Chu, H. B.; Li, Y.; Liu, J. *Nano Res.* **2009**, *2*, 903–910.
(55) Berber, S.; Oshiyama, A. *Phys. Rev. Lett.* **2006**, *96*, 105505.
(56) Ishigami, N.; Ago, H.; Imamoto, K.; Tsuji, M.; Iakoubovskii, K.; Minami, N. *J. Am. Chem. Soc.* **2008**, *130*, 9918–9924.
(57) Soares, J. S.; Barboza, A. P. M.; Araujo, P. T.; Barbosa Neto, N. M.; Nakabayashi, D.; Shadmi, N.; Yarden, T. S.; Ismach, A.; Geblinger, N.; Joselevich, E.; Vilani, C.; Cançado, L. G.; Novotny, L.; Dresselhaus, G.; Dresselhaus, M. S.; Neves, B. R. A.; Mazzoni, M. S. C.; Jorio, A. Submitted for publication.
(58) Scharifker, B. R.; Hills, G. *Electrochim. Acta* **1983**, *28*, 879–889.
(59) Scharifker, B. R.; Mostany, J. *J. Electroanal. Chem.* **1984**, *177*, 13–23.
(60) Matthijs, E.; Langerock, S.; Michailova, E.; Heerman, L. *J. Electroanal. Chem.* **2004**, *570*, 123–133.
(61) Mazaira, D.; Borrás, C.; Mostany, J.; Scharifker, B. R. *J. Electroanal. Chem.* **2009**, *631*, 22–28.
(62) Sun, Y.; Liu, Y. W.; Liang, Z. X.; Xiong, L.; Wang, A. L.; Chen, S. L. *J. Phys. Chem. C* **2009**, *113*, 9878–9883.
(63) Landolt, D. *J. Electrochem. Soc.* **2002**, *149*, S9–S20.
(64) Singh, M. P.; Bhandari, C. M. *Solid State Commun.* **2003**, *127*, 649–654.
(65) Li, L.; Yang, Y. W.; Huang, X. H.; Li, G. H.; Zhang, L. D. *Nanotechnology* **2006**, *17*, 1706–1712.
(66) Martín-González, M. S.; Prieto, A. L.; Gronsky, R.; Sands, T.; Stacy, A. M. *J. Electrochem. Soc.* **2002**, *149*, C546–C554.
(67) Gu, X.; Shadmi, N.; Cohen, H.; Joselevich, E. To be submitted for publication.

DOI: 10.1021/nl103270s | *Nano Lett.* **2010,** *10,* 4742-–4749

Supporting Information

"Drawing with nanotubes": Creating nanowires with complex geometries by pulsed electrodeposition on self-organized carbon nanotube patterns

*Tohar S. Yarden and Ernesto Joselevich**

Department of Materials and Interfaces, Weizmann Institute of Science, Rehovot 76100, Israel

Materials & Methods

Nanotube Growth

The substrate we used for growing nanotubes as parallel line arrays, serpentines and coils was miscut quartz (vicinal α-$SiO_2(1\bar{1}01)$, Y-cut singly rotated about the X-axis at an angle of $35^0$30', purchased from Roditi Intl., London, and Krystaly, Hradec Králové). To allow real-time observation of experiments under an optical microscope, we used double-side polished wafers, which are transparent (see experimental setup on Figure 1). Quartz substrates (8 × 8 × 0.5 mm) were annealed in air at 900 ^{0}C for 8 hrs. The catalyst

*Corresponding author: ernesto.joselevich@weizmann.ac.il

for chemical vapor deposition (CVD) was Fe nanoparticles. These were deposited on the substrate by one of the following methods: (i) Deposition of ferritin from solution: 0.1 g/l aqueous solution of ferritin type I from horse spleen (Sigma-Aldrich) was deposited on each sample for ~10 min. Samples were then rinsed with deionized water (Simplicity 185 purifier from Millipore, resistivity 18.2 MΩ·cm) and blow-dried with N_2. The ferritin was then oxidized by oxygen plasma (March Plasmod GCM 200, 1 sccm of O_2 for 3 min., at 100W). This was the usual procedure for growing surface-aligned nanotube arrays. (ii) Electron-beam evaporation: Fe (Kurt J. Lesker, 99.95%) is evaporated by e-beam (Odem scientific applications, initial vacuum ~$1.0x10^{-5}$ mbar) to a nominal thickness of 2 Å. Evaporated Fe was usually used for growth of serpentines and coils. For this purpose, it was deposited onto a pattern of amorphous silica (SiO_2 from Kurt J. Lesker, 99.99%) prepared by photolithography and electron-beam evaporation.

For CVD, samples were placed inside a quartz tube (fused silica; outer diameter 2.5 cm, inner diameter 2.2 cm) and aligned such that surface steps are either parallel to the gas-flow along the tube (for growth of nanotube arrays) or at some angle to it (usually 90^0, for growth of serpentines and coils). The tube was placed in a furnace (Lindberg Blue). Samples with evaporated Fe were first oxidized, either for 90 min. at 900 ^{0}C (for growth of nanotube arrays) or for 20 min. at 550 ^{0}C (for growth of serpentines and coils). CVD was performed either at 854 ^{0}C (for ferritin catalyst) or at 900 ^{0}C (for evaporated Fe catalyst), in a mixture of 60% Ar (99.998%, Oxygen & Argon Industries), 40% H_2 (99.999%, Gordon Gas) and 0.2% ethylene (99.9%, Gordon Gas). Total flow rates were either 500 or 1000 sccm, and growth times were between 45 and 90 min. A flow rate of

2000 sccm was used once in order to produce straight, flow-aligned nanotubes perpendicular to the quartz steps.

Electrochemical Setup

The electrochemical setup is a specially-prepared electrochemical cell (Figure 1). Experiments can be observed under an optical microscope in real-time, since both the cell's base and cover are transparent. The cell's volume is approximately 50 μL. The working electrode (WE) is composed of the nanotubes grown on quartz samples. Electrical contact with the nanotubes was provided by Ti electrodes. Ti was deposited over the catalyst pattern by photolithography and electron-beam evaporation (Kurt J. Lesker, 99.995%; thickness 40 nm). Quartz samples carrying carbon nanotubes and Ti contacts were then used as the cover of the electrochemical cell. The counter electrode (CE) is 100 nm-thick Au (Kurt J. Lesker, 99.999%) patterned on a glass slide that serves as the cell's base. Counter electrodes were fabricated by photolithography and e-beam evaporation, using 5 nm-thick Cr (Kurt J. Lesker, 99.95%) or Ti as an adhesive layer. The cell compartment is carved from a cast slab of polydimethylsiloxane, 1-2 mm-thick (PDMS; 184 Silicone Elastomer Kit, Sylgard, 10:1 elastomer:curing agent). The PDMS provides good sealing of the cell at both base and cover. As a pseudo-reference electrode (RE), we use Ag wire (0.1 mm diameter, 99.9% from Sigma-Aldrich). The wire is suspended across the cell by sewing it through the PDMS slab, and then oxidized to Ag/AgCl. All potentials mentioned in this work are defined vs. this reference.

Solutions were prepared using the following salts: $HAuCl_4$ (99.999%, Sigma-Aldrich), KCl (99.5%, Merck), $BiNO_3 \cdot 5H_2O$ (99.999%, Sigma-Aldrich), TeO_2 (99.9995%, Sigma-Aldrich). Nitric acid (HNO_3 65%, pro analysi, Merck). Electrodeposition of Au was

performed from a solution of $HAuCl_4$ 0.24 mM, with KCl 0.1 M as the supporting electrolyte. Electrodeposition of Bi_2Te_3 was performed from a solution of $BiNO_3$ 5 mM, TeO_2 6.67 mM, with HNO_3 1.6 M as the supporting electrolyte. Solutions were bubbled with Ar prior to experiments. Experiments were performed at room temperature.

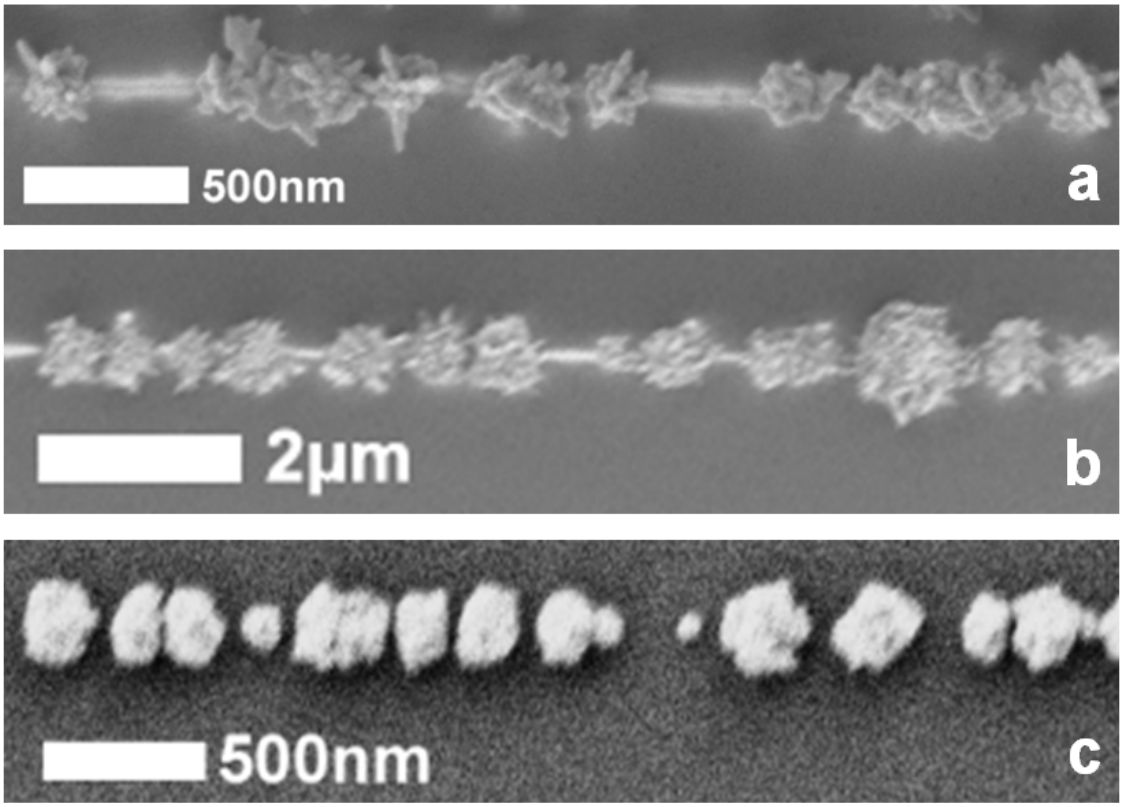

Figure S1. Morphologies of Au nanoparticles on surface-aligned carbon nanotubes. Deposition is performed by applying single potential steps: (a) -0.2 V, 10 s. (b) -1.0 V, 10 s. (c) -1.3 V, 10 s. (a) and (b) are SEM image taken on the in-lens detector, showing the underlying nanotube as a white glow. Deposited material is rough, suggesting a process of diffusion-limited aggregation. The image in (c) was taken with the SE2 lateral (Everhart–Thornley) secondary electron detector, and shows smoother particles.

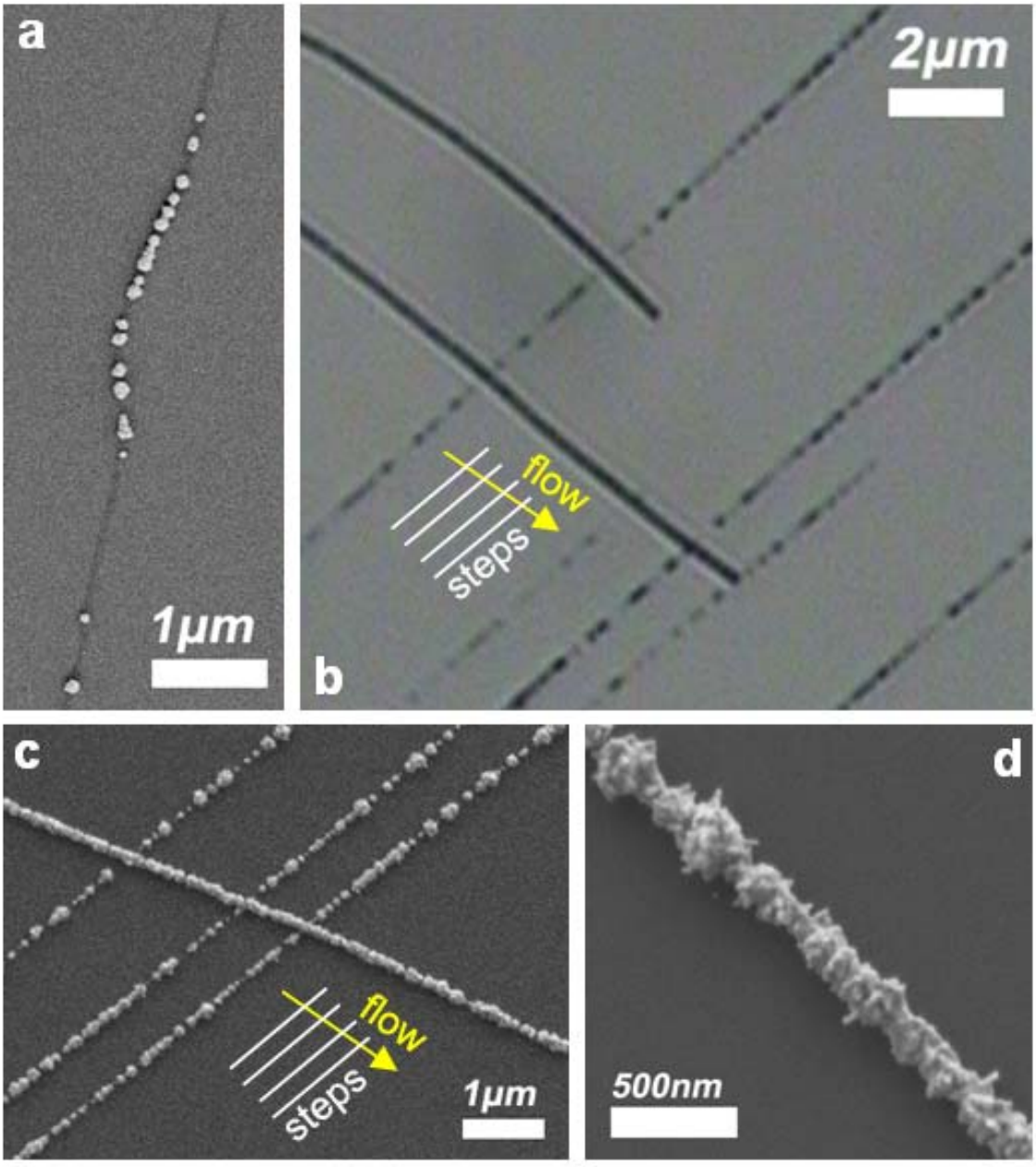

Figure S2. Effect of surface alignment on electrodeposition. (a) A surface-aligned nanotube gone "off-track", showing denser Au deposition on its deviating section (following a -1.6 V, 1 s potential step). This pattern of nucleation was commonly observed in potential step experiments. The image mixes data from both the in-lens and SE2 detectors of the SEM. (b) Optical (transmission) image of flow- and surface-aligned

nanotubes electrodeposited with Au by application of -1.6 V for 10 s (flow marked in yellow, surface steps in white). (c) SEM image taken from the same sample as (b), confirming that flow-aligned nanotubes exhibit a higher particle density following the potential step, and are continuously covered by metal. (d) SEM close-up image showing the typical morphology of deposit on flow-aligned nanotubes following a potential step of -1.6 V, 10 s.

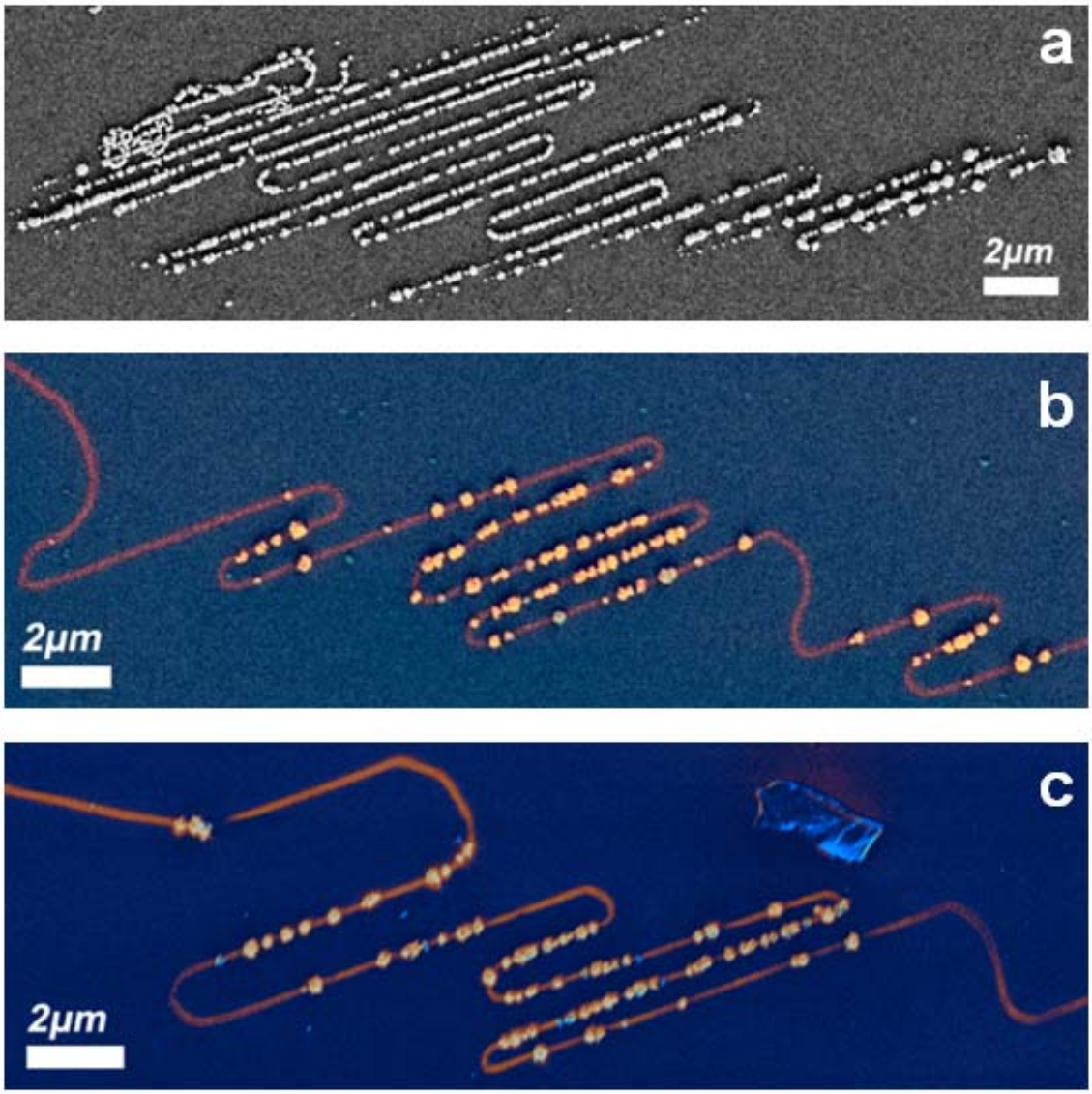

Figure S3: Effect of surface alignment on electrodeposition along nanotube serpentines. Following a single potential step of -1.6 V, 2 s, some serpentines show uniform

decoration by Au nanoparticles (a) while in others, decoration appears to be selective to straight, surface step-aligned segments (b,c). (a) is an SE2 detector SEM image; (b) and (c) mix data from both in-lens and SE2 detectors, also in different color channels, to show the nanotube serpentine in red and deposited nanoparticles in yellow.

Discussion on the current transients for more negative applied potentials

The current transients recorded at surface-aligned nanotube arrays for more negative (< -0.8 V) applied potentials show a marked deviation from the theoretical curves of both the instantaneous and progressive nucleation mechanisms.[1,2] Furthermore, they do not show the Cottrellian decay of $t^{-1/2}$ expected at long times even after 10 s of applied constant potential ($t/t_{max} \sim 100$). The decay of these current transients is much slower (around $t^{-1/7}$), and quite similar to those reported for electrodeposition of Ag on random nanotube networks[3] and Ni on nanotube forests.[4] The Scharifker-Mostany model (of which the instantaneous and progressive nucleation curves are limiting cases) was shown to be inaccurate, especially in the case of progressive nucleation.[5,6] Nevertheless, its shortcomings cannot account for the qualitatively different decay mentioned above. We propose that the non-Cottrellian decay reported here and in the said works for electrodeposition on nanotubes may be attributed to one or more of the following factors:

(i) The inherent anisotropy of surface-aligned arrays: At more negative potentials, the nucleation density along each nanotube is significantly higher than the density in any other direction. Thus, the dense nucleation induced by more negative potentials could change the pattern of overlap of exclusion zones and the rate at which diffusion zones cover the sample surface. The former controls the saturation in nucleation density and the latter affects the rate of current decay (its approach to the Cottrell curve). Thus,

nucleation could be arrested as exclusion zones come to cover the nanotubes, though diffusion zones have not yet reached the total area predicted by the two-dimensional form of the Kolmogorov-Avrami theorem (e.g. due to their "clustering" in rows along nanotubes, leaving much area for expansion between their rows). This could explain an early current peak (brought about by the virtual arrest of nucleation) and a subsequent slow decay (since the diffusion zones are late in spreading over the whole surface). Effectively, the situation described above may be viewed as introducing a transitional phase of hemicylindrical or band diffusion to multiple electrodes. This phase should succeed the initial hemispherical diffusion to individual nuclei, and be replaced by the late linear diffusion that evolves with total coverage by diffusion zones. Diffusion to regularly spaced arrays of hemicylindrical electrodes allows lower current densities compared to diffusion to a planar electrode of equivalent area.[7] The reduction in current efficiency depends on electrode size and spacing. It follows that different applied potentials, which result in different rates of nucleation and growth, should have different effects on the current efficiency (e.g. a more negative potential would make the reduction current transient at a sparse array similar to that of a dense array at a less negative potential). A similar situation may be happening in our randomly-spaced arrays, limiting the current to an extent that changes with time. The current peak may therefore be lower than predicted by two-dimensional multiple nucleation theory, and its decay slower as the inhibition due to the array structure is gradually relieved and planar diffusion becomes more dominant.

(ii) Non-planar diffusion to nanotube arrays: In nanoelectrode ensembles (i.e. arrays with non-regular spacing), different experimental parameters produce different

diffusional regimes.[8-11] Application of highly negative potentials could perhaps give rise to patterns other than planar diffusion to the array as a whole. Examples include hemicylindrical or planar diffusion to each individual nanotube (after merging of the diffusion zones of nuclei on each nanotube). These would be analogous to the results of high sweep rates in voltammetry of nanoelectrode ensembles. The resulting current profiles would undoubtedly be very different from those formulated for nucleation on surfaces. Note that the explanation of non-planar diffusion may have consequences similar to that of anisotropy, but could equally apply to random nanotube networks.

(iii) Electron-transfer limitations: Low electron-transfer rates during the initial phase of the current transient (i.e. when most of the nucleation occurs),[12] or either during the whole potential step, could result in current peaks lower than the maximum current allowed by diffusion limitations, invalidating the comparison between dimensionless transients and the Scharifker curves. The same could result from mass-transport rates that are higher than usual, for example in the early stages of particle growth. There is currently no theoretical treatment of electrodeposition reactions under mixed control. However, since electron-transfer rates should increase as potentials become more negative, we deem this factor less likely to account for the anomalous profile of current transients. Still, certain applied potentials may result in small overlap between electrode and reactant states due to a shift in the whole band-structure of the nanotube electrode. In carbon nanotubes, applied potentials mainly shift the Fermi level, but strong potentials could also shift the electronic band-structure.[13,14] The density of states (DOS) of nanotubes consists of van Hove singularities separated by intervals of low DOS, with a bandgap for semiconducting nanotubes. Thus, if an applied potential brings the bandgap,

or even a low-DOS region, of the band-structure near the reactant states, there will be only a small overlap of energy states, which leads to a low rate of electron-transfer.[15]

(iv) Nanoelectrode effects: Diffusion-controlled reactions at nanoelectrodes often show deviations from classical behavior. This is attributed to the overlap of the concentration depletion layer with the electrical double-layer. Specifically, anion reduction (as is the case in our Au deposition reaction) is inhibited. The effect should be noticeable only at the smallest nanoelectrodes, as are our 1-5 nm-diameter nanotubes. Also, in the presence of a supporting electrolyte, the deviations from classical theory should not exceed 20%.[16] Thus, currents at the initial phase of the transient (where most nucleation takes place, i.e. the reaction occurs mainly at very small nanoelectrodes) may be lower than predicted by theory. This effect would be similar to that described for electron-transfer limitations (iii).

There may be ways to determine which of the possible reasons given above is at work in moderating the current decay at more negative potentials. For example, comparing the transients recorded for nanotube arrays and random networks may elucidate the role of anisotropy. The role of diffusion regimes could be assessed by recording transients for arrays of different nanotube densities: Denser arrays may exhibit planar diffusion even for highly negative potential steps, indicating that non-planar diffusion is part of the reason for unusual current transients. Finally, deposition from a different Au species, e.g. a cationic one, could refute or lend support to the assumption that nanoscale effects at the nanotube electrodes are at work, inhibiting reduction and decreasing currents.

Supporting References

1. Scharifker, B. R.; Hills, G. *Electrochim. Acta* **1983**, *28*, 879-889.

2. Scharifker, B. R.; Mostany, J. *J. Electroanal. Chem.* **1984**, *177*, 13-23.

3. Day, T. M.; Unwin, P. R.; Wilson, N. R.; Macpherson, J. V. *J. Am. Chem. Soc.* **2005**, *127*, 10639-10647.

4. Tamburri, E.; Toschi, F.; Guglielmotti, V.; Scatena, E.; Orlanducci, S.; Terranova, M. L. *J. Nanoparticle Res.* **2009**, *11*, 1311-1319

5. Matthijs, E.; Langerock, S.; Michailova, E.; Heerman, L. *J. Electroanal. Chem.* **2004**, *570*, 123-133.

6. Mazaira, D.; Borras, C.; Mostany, J.; Scharifker, B. R. *J. Electroanal. Chem.* **2009**, *631*, 22-28.

7. Morf, W. E. *Anal. Chim. Acta* **1996**, *330*, 139-149.

8. Penner, R. M.; Martin, C. R. *Anal. Chem.* **1987**, *59*, 2625-2630.

9. Hulteen, J. C.; Menon, V. P.; Martin, C. R. *J. Chem. Soc., Farady Transactions* **1996**, *92*, 4029.

10. Koehne, J.; Li, J.; Cassell, A. M.; Chen, H.; Ye, Q.; Ng, H. T.; Han, J.; Meyyappan, M. *J. Mater. Chem.* **2004**, *14*, 676-684.

11. Arrigan, D. W. M. *Analyst* **2004**, *129*, 1157-1165.

12. Abyaneh, M. Y. *J. Electroanal. Chem.* **2006**, *586*, 196-203.

13. Heller, I.; Kong, J.; Williams, K. A.; Dekker, C.; Lemay, S. G. *J. Am. Chem. Soc.* **2006**, *128*, 7353-7359.

14. Kalbac, M.; Farhat, H.; Kavan, L.; Kong, J.; Sasaki, K.-i.; Saito, R.; Dresselhaus, M. S. *ACS Nano* **2009**, *3*, 2320-2328.

15. Bard, A. J.; Faulkner, L. R., *Electrochemical Methods: Fundamentals and Applications*. John Wiley & Sons: New York, NY, 2001.

16. Sun, Y.; Liu, Y.; Liang, Z.; Xiong, L.; Wang, A.; Chen, S. *J. Phys. Chem. C* **2009**, *113*, 9878-9883.